

PARALLEL NAVIGATION FOR 3-D AUTONOMOUS VEHICLES

SHULIN FENG, SHUNING ZHANG, MINGMING XU AND GUANLONG DENG

In this paper, parallel navigation is proposed to track the target in three-dimensional space. Firstly, the polar kinematics models for the vehicle and the target are established. Secondly, parallel navigation is derived by using polar kinematics models. Thirdly, cell decomposition method is applied to implement obstacle avoidance. Fourthly, a brief study is given on the influence of uncertainties. Finally, simulations are conducted by MATLAB. Simulation results demonstrate the effectiveness of the parallel navigation.

Keywords: parallel navigation, track, obstacle avoidance, uncertainties

Classification: 93C85

Nomenclature

(X_I, Y_I, Z_I)	reference coordinate system
(X_V, Y_V, Z_V)	coordinate system of vehicle body
(X_G, Y_G, Z_G)	coordinate system of target body
(X_L, Y_L, Z_L)	line of sight (LOS) coordinate system
$v_V (v_G)$	vehicle (target) velocity
ρ_{GV}	distance between vehicle and target
L_{GV}	LOS of vehicle-target
ξ_L, ϑ_L	pitch angle and yaw angle of L_{GV}

1. INTRODUCTION

Parallel navigation principle was first applied in the Lark missiles. Currently, parallel navigation is used mostly at the homing stage [14]. Several solutions have been used in this study. The algorithm of [1] is under geometrical constraints, where the goalkeeper moves on lines which are parallel to the initial line. The control method of [2] is under parallel navigation where the goalkeeper moves on lines which are parallel to the initial LOS. In [3], a method is proposed for robot navigation toward the moving goal. In [13], bats can track diving mantises by using parallel navigation. In [22], the subnetwork integrates information from parallel subnetworks and forecasts the pose of the agent.

As studied in [11], the time-optimal paths of the parallel navigation are geodesics of a finsler metric. The proposed guidance method of [21] can improve the effectiveness of the proportional navigation law against maneuvering targets. In [7], the trajectory equation of multi-ship navigation is studied, and the trajectory of the replenishment ship is controlled by the synchronization control algorithm. The paper of [9] gives analysis based on a parallel navigation time domain scheme. For multi-ship parallel navigation of [16], the accuracy of navigation is low due to the failure to distinguish the course in the calculation. In [12], a strategy for cable-driven parallel robots is proposed by using simplified analysis. In [10], an adaptive controller is given for parallel robots by using the Jacobian matrix. The paper of [8] designs a robust control scheme for a cable-driven parallel robot. The application of parallel navigation requires improvements. The presentation of this paper is different from the classical presentation. Parallel navigation is proposed by using the flight path and heading angles of the vehicle. This presentation is more proper for the vehicle than the classical presentation, where parallel navigation is proposed in accordance with lateral and vertical acceleration. Proportional navigation presents a family of navigation laws resulting in a rich behavior. Then, the presentation of proportional navigation is easily adapted to collision avoidance, and proportional navigation is written as a function of the flight path and heading angles. In this paper, our aim is to contribute to the method of tracking by vehicle and target. This method belongs to the family of classical guidance laws, which are based on the synthesis of kinematics equations with geometric constraints.

As studied in [3], an approximate cell decomposition approach is used to implement obstacle avoidance. In [5], the EDP polygonal approximation algorithm and cell decomposition are given for robot path-planning with curvilinear obstacles. The pursuit method of [15] is under geometrical constraint parallel navigation, applying this principle to track the target and for evading obstacles. In the study of [20], motion planning for simultaneous obstacle avoidance and target tracking is proposed in the complex workspace. In [4], cell decomposition technique which is known as one of the combinatorial methods can be represented with configuration space. By the study above, this method is simple and can be easily integrated with parallel navigation. In this paper, approximate cell decomposition combined with parallel navigation is designed to track the target and for evading obstacles. As studied in [3], the authors propose the result on the influence of uncertainties. The approach of [6] fuses measurements of differing reliability, and this architecture is flexible to the addition of new nodes and, to a certain extent, robust to node or communication link failures. The article of [17] studies the fault-tolerant control problem for stochastic switched interval time-delayed uncertain systems, which can avoid uneasy measurement on the time derivative. In [18], the state observer is applied to estimate both the unmeasurable system states and acting lumped disturbance. The paper of [19] studies the command filtered backstepping synchronization control method, and adaptive control is applied to compensate the torque disturbance. By the study above, state estimation can deal with the influence of uncertainties. In this paper, real-time state estimation is applied to cope with the uncertainties the motion attitude of target.

In the study of [3], the method is based on parallel navigation. Then, the robot moves in lines that are parallel to the initial LOS. In [3], uncertainties in the position and the

LOS angle have been taken into account, and obstacle-avoidance mode is implemented in parallel navigation. In spite of the method of [3] seeming to be quite competent, it sustains the following drawbacks.

1. The control law for robot steering angle need to continue to be expanded.
2. The estimation method for uncertainties need to be expanded.
3. Algorithm of obstacle avoidance need to be designed under obstacle-avoidance mode.

The pursuit method given in this paper is based on parallel navigation, which can track the target and for evading obstacles and uncertainties in three-dimensional space. The control objective of this paper is to implement parallel navigation and obstacle avoidance using valid model-based method. It can be applied to both online and offline navigation and obstacle avoidance. This method consists of a family of methods for vehicle navigation under parallel navigation, where this paper applies the vehicle kinematics equations combined with geometric constraints. This method is famous for the robustness. The challenge of this paper is how to propose control law for parallel navigation and implement obstacle avoidance and state estimation. To cope with the challenge, this paper presents the polar kinematics models of vehicle-target. The control law of parallel navigation is given based on the flight path and heading angles for the vehicle. Cell decomposition method need to be effectively defined as a finite collection of cells, and state estimation is applied to give a reasonable mode for calculating on the influence of uncertainties.

The method of this paper is compared with the conventional guidance laws such as pure proportional navigation (PPN) guidance law and also evolutionary strategy inspired by parallel navigation guidance law. The main difference between parallel navigation and proportional navigation is that parallel strategy keeps the pitch angle and yaw angle constant.

The contribution consists of a family of navigation laws for an autonomous vehicle. The advantages can be formulated as follows.

1. The method can define non-straight paths to the target. These paths can implement to avoid obstacles and overcome uncertainty, and satisfy the constraint on the motion of the vehicle.
2. The method proposes a family of navigation laws resulting in a rich behavior for different control laws.
3. The method gives thought to online response, where the path of the vehicle can be varied online by transforming parameters.

The remainder of this paper is organized as follows. Section 2 proposes kinematics model. The parallel navigation is deduced in Section 3. Collision avoidance can be implemented in Section 4. Section 5 proposes state estimation method in the presence of uncertainty. A series of simulation results are given in Section 6. Finally, Section 7 concludes this paper.

2. KINEMATICS MODELING

Consider Figure 1 in which a 3-D workspace is attached to a reference coordinate system. The vehicle V is moving in the workspace, and the target G moves with unknown maneuvers in the 3-D space. This paper applies the polar representation to derive the kinematics equations between the vehicle and the target in the three-dimensional space. For the vehicle, v_V is speed of the vehicle, μ_V and ϖ_V are the flight path and heading angles. v_V, μ_V, ϖ_V are the control input. For the target, v_G is speed of the target, μ_G and ϖ_G denote the flight path and heading angles. LOS of vehicle-target is denoted by L_{GV} . ξ_L and ϑ_L are the pitch angle and yaw angle of L_{GV} . ϱ_{GV} denotes the relative distance of vehicle-target.

In the reference coordinate system, the vehicle moves with

$$\begin{cases} \dot{x}_V = v_V \cos \mu_V \cos \varpi_V \\ \dot{y}_V = v_V \cos \mu_V \sin \varpi_V \\ \dot{z}_V = v_V \sin \mu_V. \end{cases} \quad (1)$$

For the target,

$$\begin{cases} \dot{x}_G = v_G \cos \mu_G \cos \varpi_G \\ \dot{y}_G = v_G \cos \mu_G \sin \varpi_G \\ \dot{z}_G = v_G \sin \mu_G. \end{cases} \quad (2)$$

The vehicle need to meet the dynamic constraints

$$\begin{cases} 0 < v_{min} < v_V < v_{max} \\ -M_1 \leq \dot{\mu}_V \leq M_1 \\ -M_2 \leq \dot{\varpi}_V \leq M_2, \end{cases} \quad (3)$$

where v_{min}, v_{max} are the minimum and maximum velocity. M_1, M_2 are numbers direct at the type of the vehicle characterizing the restrictions on the flight path and heading angles.

In this paper, the differential equations for the range ϱ_{GV} , the pitch angle of L_{GV} and the yaw angle of L_{GV} are

$$\begin{cases} \dot{\varrho}_{GV} = v_G \cos \mu_G \cos \varpi_G - v_V \cos \mu_V \cos \varpi_V \\ \varrho_{GV} \dot{\xi}_L = v_G \sin \mu_G - v_V \sin \mu_V \\ \varrho_{GV} \cos \xi_L \dot{\vartheta}_L = v_G \cos \mu_G \sin \varpi_G - v_V \cos \mu_V \sin \varpi_V. \end{cases} \quad (4)$$

In this paper, the aim is to implement the parallel navigation strategy for tracking to minimize the distance between the vehicle and the target at the interception time. Based on the the polar kinematics models, the parallel navigation strategy is discussed in the next section.

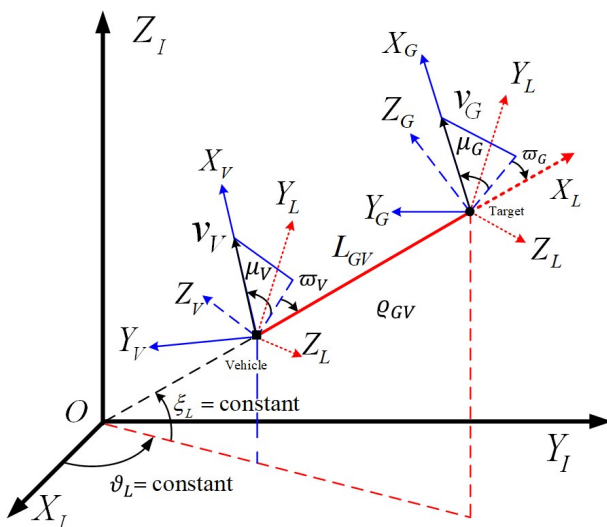


Fig. 1. Parallel navigation for vehicle-target.

3. PARALLEL NAVIGATION STRATEGY

The strategy is based on the parallel navigation, where this guidance strategy integrates the polar kinematics models of vehicle-target with geometric constraints. Based on the parallel navigation, the vehicle can reach the target in a rendezvous course. It can be implemented by controlling the pitch angle and yaw angle of L_{GV} to the constant value.

Based on parallel navigation strategy, it yields that

$$\begin{cases} \xi_L = constant \\ \vartheta_L = constant. \end{cases} \tag{5}$$

Thus, the vehicle can move in lines that are parallel to the initial LOS. In view of the pitch angle and yaw angle of L_{GV} is constant value, one can have

$$\begin{cases} \dot{\xi}_L = 0 \\ \dot{\vartheta}_L = 0. \end{cases} \tag{6}$$

From the second and third expression in (4), one can get

$$\begin{cases} \sin \eta_V = \frac{v_G}{v_V} \sin \eta_G \\ \sin \varpi_V \cos \mu_V = \frac{v_G}{v_V} \cos \mu_G \sin \varpi_G. \end{cases} \tag{7}$$

The result given in (7) gives the relationship between (v_V, η_V, ϖ_V) and (v_G, η_G, ϖ_G) , then the vehicle is in a rendezvous course with the moving target.

Considering the feasibility of the control strategy, the following assumptions are given in this paper.

Assumption 1. The vehicle is faster than the moving target, i. e., $-v_V < v_G < v_V$.

Assumption 2. The radial velocity component of the vehicle is greater than zero.

Assumption 3. The vehicle has sensory systems that allow to measure pose states information of the target, and the vehicle receives the commands of sensory systems to track the target.

In the sequel, the main result of parallel navigation is proved in the following theorem.

Theory 3.1. Based on the Assumption 1, 2, 3 and (7), the vehicle can reach the moving target in 3-D coordinate system.

Proof. To prove this theory, it need deduce that $\dot{\rho}_{TR} < 0$. The proof is based on the following remarks. Based on (7), it yields that

$$\begin{aligned}
 & v_G^2 \cos^2 \eta_G \cos^2 \varpi_G - v_V^2 \cos^2 \eta_V \cos^2 \varpi_V \\
 &= v_G^2 \cos^2 \eta_G \cos^2 \varpi_G - v_V^2 \cos^2 \eta_V (1 - \sin^2 \varpi_V) \\
 &= v_G^2 \cos^2 \eta_G \cos^2 \varpi_G - v_V^2 \cos^2 \eta_V + v_V^2 \cos^2 \eta_V \sin^2 \varpi_V \\
 &= v_G^2 \cos^2 \eta_G \cos^2 \varpi_G - v_V^2 \left(1 - \frac{v_G^2}{v_V^2} \sin^2 \eta_G\right) + v_V^2 \cos^2 \eta_V \sin^2 \varpi_V \\
 &= v_G^2 \cos^2 \eta_G \cos^2 \varpi_G - v_V^2 + v_G^2 \sin^2 \eta_G + v_G^2 \cos^2 \eta_G \sin^2 \varpi_G \\
 &= v_G^2 \cos^2 \eta_G + v_G^2 \sin^2 \eta_G - v_V^2 = v_G^2 - v_V^2.
 \end{aligned} \tag{8}$$

Based on the Assumption 1, one has

$$v_G^2 \cos^2 \eta_G \cos^2 \varpi_G - v_V^2 \cos^2 \eta_V \cos^2 \varpi_V < 0. \tag{9}$$

Under the Assumption 2, one can obtain

$$v_V \cos \eta_V \cos \varpi_V > 0, \tag{10}$$

the following two cases will be discussed.

First case: Assuming that $v_G \cos \eta_G \cos \varpi_G \geq 0$. Based on (10), it is clear that

$$v_G \cos \eta_G \cos \varpi_G + v_V \cos \eta_V \cos \varpi_V > 0, \tag{11}$$

depending on (4), (9) and (11), it can be obtained that

$$\dot{\rho}_{GV} = \frac{v_G^2 \cos^2 \eta_G \cos^2 \varpi_G - v_V^2 \cos^2 \eta_V \cos^2 \varpi_V}{v_G \cos \eta_G \cos \varpi_G + v_V \cos \eta_V \cos \varpi_V} < 0. \tag{12}$$

Second case: Assuming that $v_G \cos \eta_G \cos \varpi_G < 0$, it can obtain

$$\dot{\rho}_{GV} = v_G \cos \eta_G \cos \varpi_G - v_V \cos \eta_V \cos \varpi_V < 0. \tag{13}$$

Based on the analysis mentioned above, one can obtain that $\dot{\rho}_{GV} < 0$ under the condition provided by (7). Based on (7), it can have the following results.

1) $v_V > 0, \eta_V, \varpi_V \in (-\frac{\pi}{2}, \frac{\pi}{2})$. According to (7), one can have

$$\begin{cases} \eta_V = \arcsin(\frac{v_G}{v_V} \sin \eta_G) \\ \varpi_V = \arcsin \frac{v_G \cos \eta_G \sin \varpi_G}{v_V \cos[\arcsin(\frac{v_G}{v_V} \sin \eta_G)]}. \end{cases} \tag{14}$$

2) $v_V > 0, \eta_V, \varpi_V \in (\frac{\pi}{2}, \frac{3\pi}{2})$. According to (7), one can have

$$\begin{cases} \eta_V = \pi - \arcsin(\frac{v_G}{v_V} \sin \eta_G) \\ \varpi_V = \pi - \arcsin \frac{v_G \cos \eta_G \sin \varpi_G}{v_V \cos[\pi - \arcsin(\frac{v_G}{v_V} \sin \eta_G)]} = \pi + \arcsin \frac{v_G \cos \eta_G \sin \varpi_G}{v_V \cos[\arcsin(\frac{v_G}{v_V} \sin \eta_G)]}. \end{cases} \tag{15}$$

3) $v_V < 0, \eta_V \in (-\frac{\pi}{2}, \frac{\pi}{2}), \varpi_V \in (\frac{\pi}{2}, \frac{3\pi}{2})$. According to (7), it yields that

$$\begin{cases} \eta_V = \arcsin(\frac{v_G}{v_V} \sin \eta_G) \\ \varpi_V = \pi - \arcsin \frac{v_G \cos \eta_G \sin \varpi_G}{v_V \cos[\arcsin(\frac{v_G}{v_V} \sin \eta_G)]}. \end{cases} \tag{16}$$

4) $v_V < 0, \eta_V \in (\frac{\pi}{2}, \frac{3\pi}{2}), \varpi_V \in (-\frac{\pi}{2}, \frac{\pi}{2})$. According to (7), it yields that

$$\begin{cases} \eta_V = \pi - \arcsin(\frac{v_G}{v_V} \sin \eta_G) \\ \varpi_V = \arcsin \frac{v_G \cos \eta_G \sin \varpi_G}{v_V \cos[\pi - \arcsin(\frac{v_G}{v_V} \sin \eta_G)]} = -\arcsin \frac{v_G \cos \eta_G \sin \varpi_G}{v_V \cos[\arcsin(\frac{v_G}{v_V} \sin \eta_G)]}. \end{cases} \tag{17}$$

This completes the proof. □

The following result relates that parallel navigation guidance law is applied in the motion. The transformation matrix between (X_I, Y_I, Z_I) and (X_L, Y_L, Z_L) is denoted by $M_{I,L}$. In the 3-D coordinate system, the kinematics equations of the vehicle are

$$\begin{pmatrix} \dot{x}_{IV} \\ \dot{y}_{IV} \\ \dot{z}_{IV} \end{pmatrix} = M_{I,L}^{-1} \begin{pmatrix} \dot{x}_{LV} \\ \dot{y}_{LV} \\ \dot{z}_{LV} \end{pmatrix} = M_{I,L}^{-1} \begin{pmatrix} v_V \cos \eta_V \cos \varpi_V \\ v_V \cos \eta_V \sin \varpi_V \\ v_V \sin \eta_V \end{pmatrix}. \tag{18}$$

Under the discrete model, transformation matrix is written by

$$M_{I,L}(\varsigma) = \begin{pmatrix} \cos \eta_L(\varsigma) \cos \varpi_L(\varsigma) & \cos \eta_L(\varsigma) \sin \varpi_L(\varsigma) & \sin \eta_L(\varsigma) \\ -\sin \varpi_L(\varsigma) & \cos \varpi_L(\varsigma) & 0 \\ -\sin \eta_L(\varsigma) \cos \varpi_L(\varsigma) & -\sin \eta_L(\varsigma) \sin \varpi_L(\varsigma) & \cos \eta_L(\varsigma) \end{pmatrix}. \tag{19}$$

In the 3-D coordinate system, the vehicle moves according to the following discrete kinematics equations

$$\begin{pmatrix} x_{IV}(\varsigma + 1) \\ y_{IV}(\varsigma + 1) \\ z_{IV}(\varsigma + 1) \end{pmatrix} = \begin{pmatrix} x_{IV}(\varsigma) \\ y_{IV}(\varsigma) \\ z_{IV}(\varsigma) \end{pmatrix} + M_{I,L}^{-1}(\varsigma) \begin{pmatrix} v_V \cos \eta_V(\varsigma) \cos \varpi_V(\varsigma) T_s \\ v_V \cos \eta_V(\varsigma) \sin \varpi_V(\varsigma) T_s \\ v_V \sin \eta_V(\varsigma) T_s \end{pmatrix}, \tag{20}$$

$$\begin{pmatrix} \eta_V(\varsigma) \\ \varpi_V(\varsigma) \\ \eta_V(\varsigma) \\ \varpi_V(\varsigma) \end{pmatrix} = \begin{pmatrix} jiao_1(\varsigma) & (v_V > 0) \\ jiao_2(\varsigma) & (v_V > 0) \\ \pi - jiao_1(\varsigma) & (v_V > 0) \\ \pi + jiao_2(\varsigma) & (v_V > 0) \end{pmatrix}, \quad (21)$$

or

$$\begin{pmatrix} \eta_V(\varsigma) \\ \varpi_V(\varsigma) \\ \eta_V(\varsigma) \\ \varpi_V(\varsigma) \end{pmatrix} = \begin{pmatrix} jiao_1(\varsigma) & (v_V < 0) \\ \pi - jiao_2(\varsigma) & (v_V < 0) \\ \pi - jiao_1(\varsigma) & (v_V < 0) \\ -jiao_2(\varsigma) & (v_V < 0) \end{pmatrix}, \quad (22)$$

where $jiao_1(\varsigma) = \arcsin[\frac{v_G(\varsigma)}{v_V(\varsigma)} \sin \eta_G(\varsigma)]$, $jiao_2(\varsigma) = \arcsin \frac{v_G(\varsigma) \cos \eta_G(\varsigma) \sin \varpi_G(\varsigma)}{v_V(\varsigma) \cos[\arcsin(\frac{v_G(\varsigma)}{v_V(\varsigma)} \sin \eta_G(\varsigma))]}$. T_s is the sampling time, and $t_\varsigma = \varsigma T_s$.

Based on (20), (21) or (22), the vehicle can reach the moving target based on the parallel navigation.

Next, given n vehicles which are expected to move in a rendezvous course. Based on the Assumption 1, 2, 3 and parallel navigation strategy, n vehicles are in a rendezvous course with the moving target. By selecting the pitch angle and yaw angle of L_{GV} flexibly, path deconfliction approached for multi-vehicle is implemented in this section. Further determines original positions, vehicle paths can not intersect under parallel navigation.

Theory 3.2. Under the Assumption 1, 2, 3 and parallel navigation strategy, n vehicles can synchronously reach the moving target in the 3-D coordinate system.

Proof. To prove this theory, it need deduce that $\dot{\rho}_{GV_i} < 0$. For the i th vehicle, $-v_{R_i} < v_G < v_{V_i}$, and the radial velocity component is that $v_{V_i} \cos \eta_{V_i} \cos \varpi_{V_i} > 0$. Under Theory 1, one can have $\dot{\rho}_{TV_i} < 0$. Then, it can have the following results.

1) When $v_{V_i} > 0$, $\eta_{V_i}, \varpi_{V_i} \in (-\frac{\pi}{2}, \frac{\pi}{2})$,

$$\begin{cases} \eta_{V_i} = \arcsin(\frac{v_G}{v_{V_i}} \sin \eta_G) \\ \varpi_{V_i} = \arcsin \frac{v_G \cos \eta_G \sin \varpi_G}{v_{V_i} \cos[\arcsin(\frac{v_G}{v_{V_i}} \sin \eta_G)]} \end{cases} \quad (23)$$

2) When $v_{V_i} > 0$, $\eta_{V_i}, \varpi_{V_i} \in (\frac{\pi}{2}, \frac{3\pi}{2})$,

$$\begin{cases} \eta_{V_i} = \pi - \arcsin(\frac{v_G}{v_{V_i}} \sin \eta_G) \\ \varpi_{V_i} = \pi + \arcsin \frac{v_G \cos \eta_G \sin \varpi_G}{v_{V_i} \cos[\arcsin(\frac{v_G}{v_{V_i}} \sin \eta_G)]} \end{cases} \quad (24)$$

3) When $v_{V_i} < 0$, $\eta_{V_i} \in (-\frac{\pi}{2}, \frac{\pi}{2})$, $\varpi_{V_i} \in (\frac{\pi}{2}, \frac{3\pi}{2})$,

$$\begin{cases} \eta_{V_i} = \arcsin(\frac{v_G}{v_{V_i}} \sin \eta_G) \\ \varpi_{V_i} = \pi - \arcsin \frac{v_G \cos \eta_G \sin \varpi_G}{v_{V_i} \cos[\arcsin(\frac{v_G}{v_{V_i}} \sin \eta_G)]} \end{cases} \quad (25)$$

4) When $v_{V_i} < 0$, $\eta_{V_i} \in (\frac{\pi}{2}, \frac{3\pi}{2})$, $\varpi_{V_i} \in (-\frac{\pi}{2}, \frac{\pi}{2})$,

$$\begin{cases} \eta_{V_i} = \pi - \arcsin(\frac{v_G}{v_{V_i}} \sin \eta_G) \\ \varpi_{V_i} = -\arcsin \frac{v_G \cos \eta_G \sin \varpi_G}{v_{V_i} \cos[\arcsin(\frac{v_G}{v_{V_i}} \sin \eta_G)]}. \end{cases} \quad (26)$$

□

4. PARALLEL NAVIGATION UNDER OBSTACLES

In the presence of obstacles, the integration of the local and the global path-planning methods is essential.

4.1. Obstacle-avoidance mode

Parallel navigation is used in combination with obstacle-avoidance. The sensory system gives the vehicle with the essential information on the obstacles and the target. Approximate cell decomposition method can be easily integrated with the parallel navigation. Originally, the vehicle navigates using the parallel navigation, and when an obstacle is detected, the obstacle-avoidance can be implemented. This method allows the combination between parallel navigation mode and the obstacle-avoidance mode.

When the obstacle is detected within a specific distance from the vehicle, obstacle avoidance is motivated, and the vehicle deviates from the nominal path to avoid obstacle. After the obstacle is passed, the vehicle regains to the navigation mode under parallel navigation.

The vehicle and the target move in the workspace with M obstacles. The vehicle path must lie in the free space. In a cell decomposition method, the workspace is broken down into independently distributed cells. The size of the cells is locally adapted to the geometry of the obstacles. The cell decomposition of workspace is defined as a finite collection of cells. The sum of all cells is the workspace, and the cells do not overlap.

4.2. Obstacle-avoidance decision

For accommodate to parallel navigation in the obstacle-avoidance mode, discrete kinematics equation of the vehicle is

$$\begin{pmatrix} x_{IV}(\zeta + 1) \\ y_{IV}(\zeta + 1) \\ z_{IV}(\zeta + 1) \end{pmatrix} = \begin{pmatrix} x_{IV}(\zeta) \\ y_{IV}(\zeta) \\ z_{IV}(\zeta) \end{pmatrix} + \lambda M_{I,L}^{-1}(\zeta) \begin{pmatrix} v_V \cos \eta_V(\zeta) \cos \varpi_V(\zeta) T_s \\ v_V \cos \eta_V(\zeta) \sin \varpi_V(\zeta) T_s \\ v_V \sin \eta_V(\zeta) T_s \end{pmatrix}, \quad (27)$$

where λ is the step size. The comprehensive method is activated after an obstacle is detected in the vehicle active region. The decision of obstacle avoidance is

- (1) Compute $[x_{IV}(\zeta + 1), y_{IV}(\zeta + 1), z_{IV}(\zeta + 1)]$ by applying (27).
- (2) Does $[x_{IV}(\zeta + 1), y_{IV}(\zeta + 1), z_{IV}(\zeta + 1)]$ fall in an empty cell?

Yes: move to $[x_{IV}(\varsigma + 1), y_{IV}(\varsigma + 1), z_{IV}(\varsigma + 1)]$, set ς as $\varsigma + 1$ and transform into (1).

No: move to the nearest empty cell to $[x_{IV}(\varsigma + 1), y_{IV}(\varsigma + 1), z_{IV}(\varsigma + 1)]$, set ς as $\varsigma + 1$ and transform into (1). The nearest empty cell is located in the direction of bit bigger than a specific distance.

(3) Stop when vehicle reaches the target.

5. PARALLEL NAVIGATION UNDER UNCERTAINTIES

The study of the navigation under uncertainty is the complicated and difficult problem. This section presents a method on the influence of uncertainties.

5.1. Uncertainty in the position, flight path and heading angles of target

Uncertainty in the position, flight path and heading angles of target is the most important part of uncertainty in the navigation. Then, odometry is applied to provide real-time position estimation of the target. According to estimated values for position, flight path and heading angles, the pose of the target is

$$X_G = [x_G, y_G, z_G, \eta_G, \varpi_G]^T. \quad (28)$$

The covariance matrix for uncertainty in pose is

$$C_G = \begin{bmatrix} \sigma_{x_G}^2 & \sigma_{x_G y_G} & \sigma_{x_G z_G} & \sigma_{x_G \eta_G} & \sigma_{x_G \varpi_G} \\ \sigma_{y_G x_G} & \sigma_{y_G}^2 & \sigma_{y_G z_G} & \sigma_{y_G \eta_G} & \sigma_{y_G \varpi_G} \\ \sigma_{z_G x_G} & \sigma_{z_G y_G} & \sigma_{z_G}^2 & \sigma_{z_G \eta_G} & \sigma_{z_G \varpi_G} \\ \sigma_{\eta_G x_G} & \sigma_{\eta_G y_G} & \sigma_{\eta_G z_G} & \sigma_{\eta_G}^2 & \sigma_{\eta_G \varpi_G} \\ \sigma_{\varpi_G x_G} & \sigma_{\varpi_G y_G} & \sigma_{\varpi_G z_G} & \sigma_{\varpi_G \eta_G} & \sigma_{\varpi_G}^2 \end{bmatrix}. \quad (29)$$

The position estimation process is activated at a regular interval Δt . Let Δl_G , $\Delta \alpha_G$ and $\Delta \beta_G$ be the change in the translation, elevation and deviation, respectively. One has

$$\Delta Z_G = \begin{bmatrix} \Delta l_G \\ \Delta \alpha_G \\ \Delta \beta_G \end{bmatrix}. \quad (30)$$

The accumulated translation, elevation and deviation are calculated as

$$\begin{cases} l_G^{new} = l_G^{old} + \Delta l_G \\ \eta_G^{new} = \eta_G^{old} + \Delta \alpha_G \\ \varpi_G^{new} = \varpi_G^{old} + \Delta \beta_G. \end{cases} \quad (31)$$

The change in pose of the target is

$$\Delta X_G = \begin{bmatrix} \Delta x_G \\ \Delta y_G \\ \Delta z_G \\ \Delta \eta_G \\ \Delta \varpi_G \end{bmatrix} = \begin{bmatrix} \Delta l_G \cos(\eta_G + \Delta \alpha_G) \cos(\varpi_G + \Delta \beta_G) \\ \Delta l_G \cos(\eta_G + \Delta \alpha_G) \sin(\varpi_G + \Delta \beta_G) \\ \Delta l_G \sin(\varpi_G + \Delta \beta_G) \\ \Delta \alpha_G \\ \Delta \beta_G \end{bmatrix} \quad (32)$$

The pose of target is estimated as follows and then updated

$$X_G^{new} = X_G^{old} + \Delta X_G. \tag{33}$$

The estimated pose of the target is accompanied by an estimate of the uncertainty expressed by C_G . The sensitivity of X_G to the observed value is denoted by the Jacobian matrix J , which is

$$J = \frac{\partial X_G}{\partial \Delta Z_G}. \tag{34}$$

Then, one can get

$$J = \frac{\partial \begin{bmatrix} \Delta x_G \\ \Delta y_G \\ \Delta z_G \\ \Delta \eta_G \\ \Delta \varpi_G \end{bmatrix}}{\partial \Delta Z_G} = \frac{\partial \begin{bmatrix} \Delta l \cos \eta_G \cos \varpi_G \\ \Delta l \cos \eta_G \sin \varpi_G \\ \Delta l \sin \varpi_G \\ \Delta \alpha_G \\ \Delta \beta_G \end{bmatrix}}{\partial \Delta Z_G} \tag{35}$$

which gives

$$J = \begin{bmatrix} \cos \eta_G \cos \varpi_G & 0 & 0 \\ \cos \eta_G \sin \varpi_G & 0 & 0 \\ \sin \varpi_G & 0 & 0 \\ 0 & 1 & 0 \\ 0 & 0 & 1 \end{bmatrix}. \tag{36}$$

J is used to denote the estimate of the position as follows:

$$X_G^{new} = X_G^{old} + J \Delta Z. \tag{37}$$

Thus, C_G is updated as follows:

$$C_G^{new} = C_G^{old} + J^T C_G^{old} J. \tag{38}$$

5.2. Uncertainty in the pitch angle and yaw angle of L_{GV}

Firstly, this section will consider uncertainty in the pitch angle of L_{GV} . The pitch angle of L_{GV} is given by

$$\tan \eta_L = \frac{z_G - z_V}{\sqrt{(x_G - x_V)^2 + (y_G - y_V)^2}}. \tag{39}$$

Let

$$g_1 = \tan \eta_L = f_1(x_G, y_G, z_G, x_V, y_V, z_V) \tag{40}$$

$$C_{I_1} = \begin{bmatrix} \sigma_{x_G}^2 & \sigma_{x_G y_G} & \sigma_{x_G z_G} & \sigma_{x_G x_V} & \sigma_{x_G y_V} & \sigma_{x_G z_V} \\ \sigma_{y_G x_G} & \sigma_{y_G}^2 & \sigma_{y_G z_G} & \sigma_{y_G x_V} & \sigma_{y_G y_V} & \sigma_{y_G z_V} \\ \sigma_{z_G x_G} & \sigma_{z_G y_G} & \sigma_{z_G}^2 & \sigma_{z_G x_V} & \sigma_{z_G y_V} & \sigma_{z_G z_V} \\ \sigma_{x_V x_G} & \sigma_{x_V y_G} & \sigma_{x_V z_G} & \sigma_{x_V}^2 & \sigma_{x_V y_V} & \sigma_{x_V z_V} \\ \sigma_{y_V x_G} & \sigma_{y_V y_G} & \sigma_{y_V z_G} & \sigma_{y_V x_V} & \sigma_{y_V}^2 & \sigma_{y_V z_V} \\ \sigma_{z_V x_G} & \sigma_{z_V y_G} & \sigma_{z_V z_G} & \sigma_{z_V x_V} & \sigma_{z_V y_V} & \sigma_{z_V}^2 \end{bmatrix} \tag{41}$$

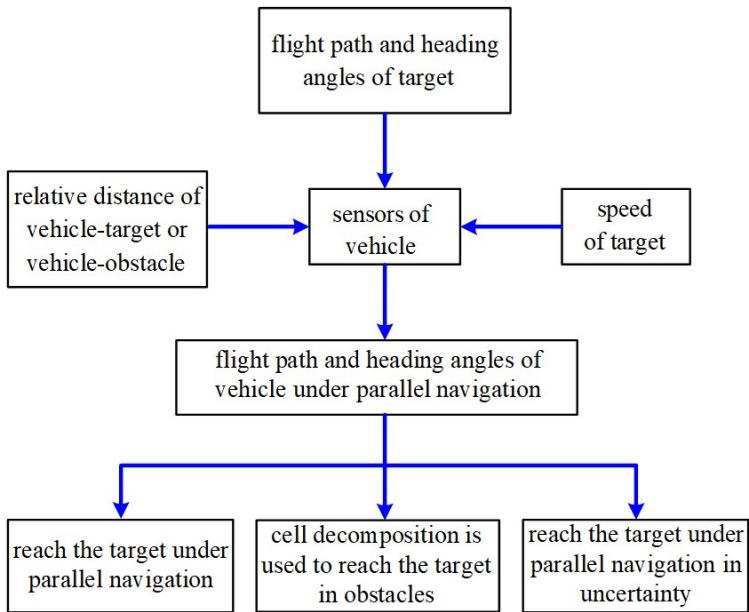


Fig. 2. Block diagram illustrating the parallel navigation.

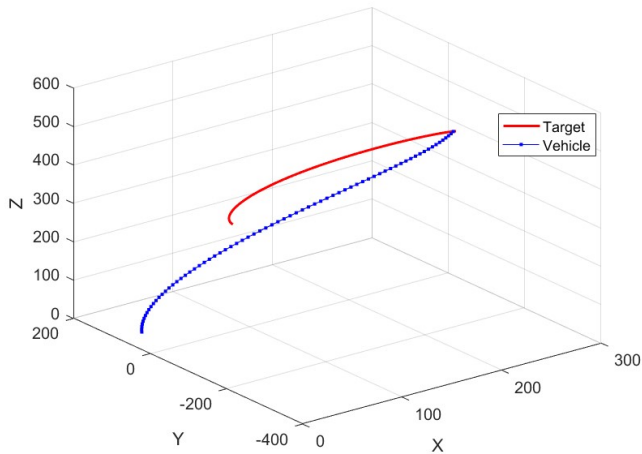


Fig. 3. The paths in Case 1 of Example 1.

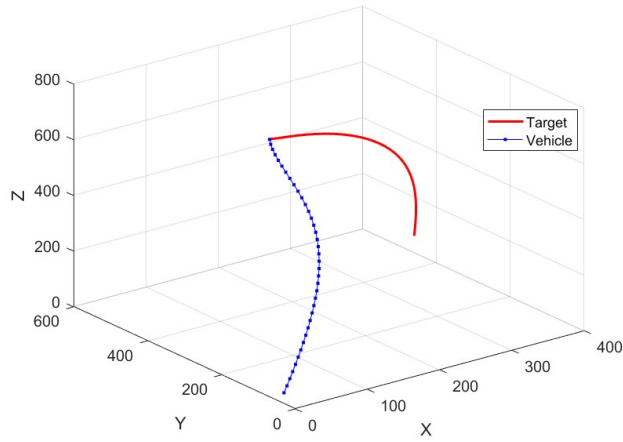


Fig. 4. The paths in Case 2 of Example 1.

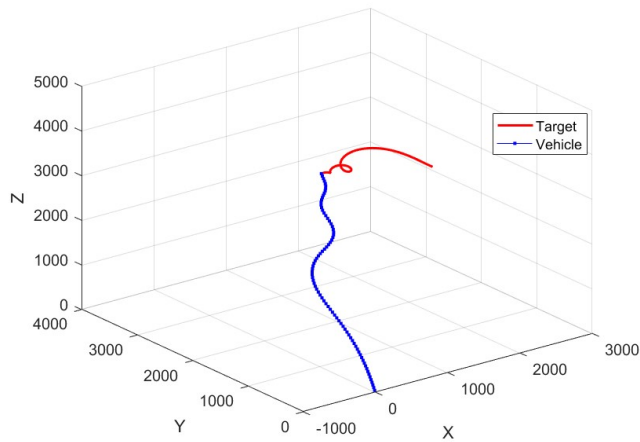


Fig. 5. The paths in Case 3 of Example 1.

Covariance matrix C_{g_1} denotes the uncertainty in the input, which is

$$C_{g_1} = \nabla f_1 C_{I_1} [\nabla f_1]^T \tag{42}$$

with

$$\nabla f_1 = \left[\frac{\partial f_1}{\partial x_G}, \frac{\partial f_1}{\partial y_G}, \frac{\partial f_1}{\partial z_G}, \frac{\partial f_1}{\partial x_V}, \frac{\partial f_1}{\partial y_V}, \frac{\partial f_1}{\partial z_V} \right]. \tag{43}$$

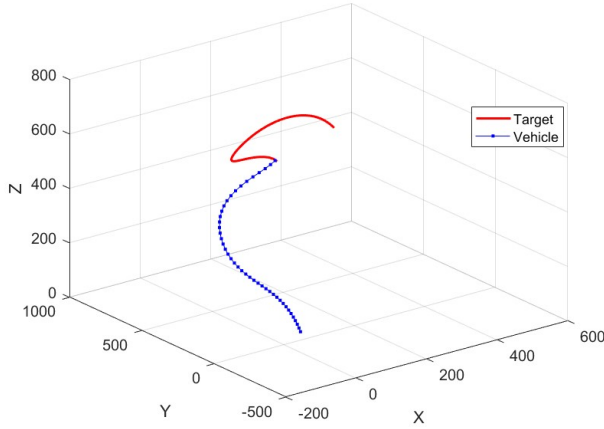


Fig. 6. The paths in Case 4 of Example 1.

Secondly, this section will consider uncertainty in the yaw angle of L_{GV} . The yaw angle of L_{GV} is given by

$$\tan \varpi_L = \frac{y_G - y_V}{z_G - z_V}. \tag{44}$$

Let

$$g_2 = \tan \varpi_L = f_2(y_G, z_G, y_V, z_V) \tag{45}$$

$$C_{I_2} = \begin{bmatrix} \sigma_{y_G}^2 & \sigma_{y_G z_G} & \sigma_{y_G y_V} & \sigma_{y_G z_V} \\ \sigma_{z_G y_G} & \sigma_{z_G}^2 & \sigma_{z_G y_V} & \sigma_{z_G z_V} \\ \sigma_{y_V y_G} & \sigma_{y_V z_G} & \sigma_{y_V}^2 & \sigma_{y_V z_V} \\ \sigma_{z_V y_G} & \sigma_{z_V z_G} & \sigma_{z_V y_V} & \sigma_{z_V}^2 \end{bmatrix} \tag{46}$$

Covariance matrix C_{g_2} denotes the uncertainty in the input, which is

$$C_{g_2} = \nabla f_2 C_{I_2} [\nabla f_2]^T \tag{47}$$

with

$$\nabla f_2 = \left[\frac{\partial f_2}{\partial y_G}, \frac{\partial f_2}{\partial z_G}, \frac{\partial f_2}{\partial y_V}, \frac{\partial f_2}{\partial z_V} \right]. \tag{48}$$

The control method given in Theory 3.1 proposes the quantities required by the guidance control for the implementation of parallel navigation. The block diagram illustrating the navigation process is shown in Figure 2. Range sensors are used to measure the distances vehicle-target and vehicle-obstacle. It can be accomplished applying LIDAR or SONAR sensors. The speed can be obtained applying velocity sensors such as Doppler LIDAR. The flight path and heading angles can be obtained applying orientation sensors. Based on the implementation, parallel navigation is proposed to implement track the

moving target, transcending the PPN in terms of interception time. The parallel navigation integrated with cell decomposition method can implement collision avoidance. Under state estimation, parallel navigation can achieve more superior tracking performance. Parallel navigation is derived assuming no delay. Communication delay are not considered in this paper, and it is the implication of the results and drawback of this specific implementation.

Control law		Eq.	Case
$v_P > 0$	$\eta_V = \arcsin\left(\frac{v_G}{v_V} \sin \eta_G\right)$	(14)	Case 1
	$\varpi_V = \arcsin \frac{v_G \cos \eta_G \sin \varpi_G}{v_V \cos[\arcsin(\frac{v_G}{v_V} \sin \eta_G)]}$		
$v_P > 0$	$\eta_V = \pi - \arcsin\left(\frac{v_G}{v_V} \sin \eta_G\right)$	(15)	Case 2
	$\varpi_V = \pi + \arcsin \frac{v_G \cos \eta_G \sin \varpi_G}{v_V \cos[\arcsin(\frac{v_G}{v_V} \sin \eta_G)]}$		
$v_P < 0$	$\eta_V = \arcsin\left(\frac{v_G}{v_V} \sin \eta_G\right)$	(16)	Case 3
	$\varpi_V = \pi - \arcsin \frac{v_G \cos \eta_G \sin \varpi_G}{v_V \cos[\arcsin(\frac{v_G}{v_V} \sin \eta_G)]}$		
$v_P < 0$	$\eta_V = \pi - \arcsin\left(\frac{v_G}{v_V} \sin \eta_G\right)$	(17)	Case 4
	$\varpi_V = -\arcsin \frac{v_G \cos \eta_G \sin \varpi_G}{v_V \cos[\arcsin(\frac{v_G}{v_V} \sin \eta_G)]}$		

Tab. 1. Four control laws of Theory 1.

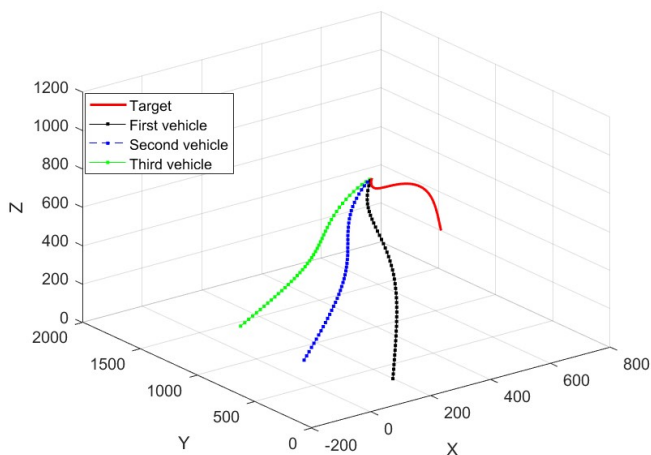


Fig. 7. Rendezvous for three vehicles.

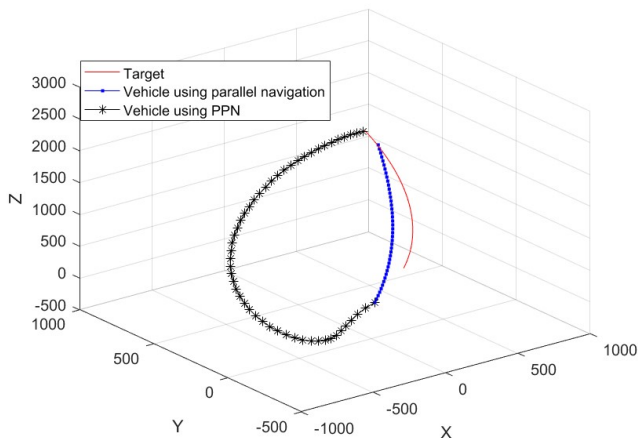


Fig. 8. Comparison with parallel navigation and PPN.

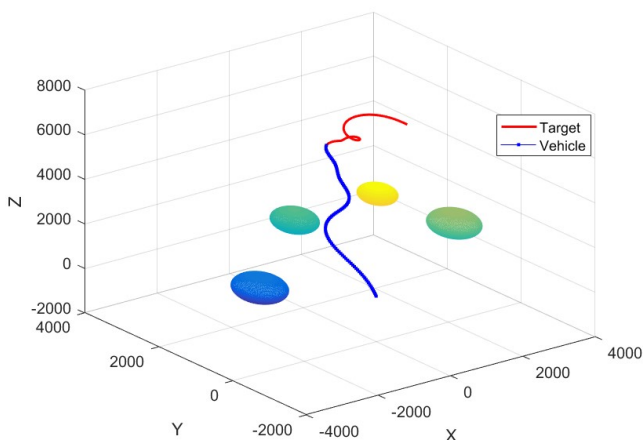


Fig. 9. Cell decomposition for spherical obstacles.

6. SIMULATION RESULTS

In this section, simulations are conducted in MATLAB environment. First, based on (14), (15), (16) and (17), parallel navigation is used to track the accelerating target. Then, comparison with the PPN is applied to reach the target. In the sequel, the cell decomposition method is applied to avoid the obstacles. Finally, under uncertainties, the parallel navigation is combined with state estimation.

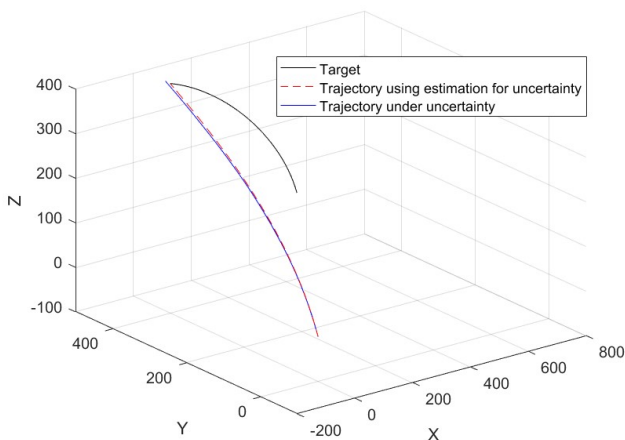


Fig. 10. Parallel navigation under uncertainties.

Example 1. In this example, the accelerating target moves with constant velocity but varying direction, and time-varying flight path and heading angles.

Based on Theory 1, Table 5.2 illustrates that the pursuer reaches the moving target under the following four cases.

Case 1: The vehicle is located at $(10m, 47m, 28m)$. The initial positions of the target is $(141m, 150m, 169m)$, and it is moving with $(\eta_G(\varsigma) = \pi/3 - \varsigma\pi/60 + (\varsigma\pi/120)^2, \varpi_G(\varsigma) = -\pi/7 + \varsigma\pi/110 - \varsigma\pi/78)$. $v_G = 6.49m/s$ and $v_V = 8.58m/s$. $\xi_L = \pi/3$ and $\vartheta_L = \pi/9$. The paths are illustrated in Figure 3, where the vehicle navigating by using (14) of Theory 1.

Case 2: The vehicle is located at $(10m, 50m, 20m)$. The initial positions of the target is $(272m, 210m, 302m)$, and it is moving with $(\eta_G(\varsigma) = \pi/10 - \varsigma\pi/130 + (\varsigma\pi/180)^2 + (\varsigma\pi/100)^4, \varpi_G(\varsigma) = \pi/20 + \varsigma\pi/110 + (\varsigma\pi/400)^2 + (\varsigma\pi/110)^3)$. $v_G = 12m/s$ and $v_V = 20m/s$. $\xi_L = \pi/3$ and $\vartheta_L = \pi/12$. The paths are illustrated in Figure 4, where the vehicle navigating by using (15) of Theory 1.

Case 3: The vehicle is located at $(11m, 30m, 20m)$. The initial positions of the target is $(3000m, 2880m, 2080m)$, and it is moving with $(\eta_G(\varsigma) = -\pi/3 + \varsigma\pi/130 - (\pi\varsigma/170)^2, \varpi_G(\varsigma) = -\pi/7 - \varsigma\pi/150 - (\varsigma\pi/110)^3)$. $v_G = 33m/s$ and $v_V = -61.3m/s$. $\xi_L = \pi/1.6$ and $\vartheta_L = -\pi/1.2$. The paths are illustrated in Figure 5, where the vehicle navigating by using (16) of Theory 1.

Case 4: The vehicle is located at $(71m, 60m, 8m)$. The initial positions of the target is $(420m, 680m, 483m)$, and it is moving with $(\eta_G(\varsigma) = \pi/4 + \varsigma\pi/210 + (\varsigma\pi/60)^2 - (\varsigma\pi/235)^3, \varpi_G(\varsigma) = -\pi/7 + \varsigma\pi/200 - (\varsigma\pi/100)^3)$. $v_G = 15m/s$ and $v_V = -20.1m/s$. $\xi_L = \pi/2.2$ and $\vartheta_L = \pi/13$. The paths are illustrated in Figure 6, where the vehicle navigating by using (17) of Theory 1.

Example 2. The three vehicles are located at $(180m, 280m, 20m)$, $(-10m, 560m, 120m)$ and $(100m, 1400m, 20m)$, respectively. $\xi_{L1} = \pi/2.4$ and $\vartheta_{L1} = \pi/12$. $\xi_{L2} = \pi/4$ and $\vartheta_{L2} = \pi/10$. $\xi_{L3} = \pi/10$ and $\vartheta_{L3} = \pi/11$. The initial positions of the target is $(272m, 100m, 802m)$, and it is moving with $(\eta_G(\zeta) = \pi/10 - \zeta\pi/130 + (\zeta\pi/180)^2 + (\zeta\pi/100)^4, \varpi_G(\zeta) = \pi/20 + \zeta\pi/110 + (\zeta\pi/300)^2 + (\zeta\pi/110)^3)$. $v_G = 11m/s$. The speeds of three vehicles are $23m/s, 19.9m/s, 19.5m/s$, respectively. The paths are illustrated in Figure 7, where three vehicles can synchronously reach the moving target by using Theory 2.

Example 3. Comparison with the PPN, and this example will be considered. The vehicle is located at $(30m, 10m, 40m)$. The initial positions of the target is $(210m, -10m, 490m)$, and it is moving with $(\eta_G(\zeta) = -25\zeta\pi/3, \varpi_G(\zeta) = 50\zeta\pi/3)$. $v_G = 29m/s$ and $v_V = 40m/s$. $\xi_L = \pi/3$ and $\vartheta_L = \pi/10$. Under PPN, the navigation constant is $N = 2.3$. The paths of vehicle-target under the parallel navigation and the PPN are shown in Figure 8, and it is observed that the pursuer navigating under the parallel navigation reaches the target before the PPN. The interception times are $t_f = 42s$ and $t_f = 50s$ for the parallel navigation and the PPN, respectively.

Example 4. At the appearance of spherical obstacles in a complicated environment, the cell decomposition algorithm is used to reach the target and avoid the obstacles. The vehicle is located at $(11m, 30m, 20m)$. The initial positions of the target is $(3790m, 2880m, 3890m)$, and it is moving with $(\eta_G(\zeta) = -\zeta\pi/3 + \zeta\pi/130 - (\zeta\pi/170)^2, \varpi_G(\zeta) = -\pi/7 - \zeta\pi/110 - (\zeta\pi/110)^2)$. $v_G = 43m/s$ and $v_V = -70m/s$. $\xi_L = \pi/1.6$ and $\vartheta_L = -\pi/1.2$. As illustrated in Figure 9, obstacle avoidance can implemented by using cell decomposition algorithm.

Example 5. This example considers uncertainties in the pitch angle and yaw angle of L_{GV} . The vehicle is located at $(0m, 0m, 0m)$. The initial positions of the target is $(171m, 191m, 220m)$, and it is moving with $(\eta_G(\zeta) = 29\zeta\pi/90, \varpi_G(\zeta) = 14.5\zeta\pi)$. $v_G = 12.8m/s$ and $v_V = 23.3m/s$. In the absence of uncertainties, $\xi_L = \pi/3.9$ and $\vartheta_L = \pi/3.1$. Figure 10 shows the paths in the presence of uncertainty, where the vehicle can reach the target by using the estimation of the pitch angle and yaw angle of L_{GV} .

7. CONCLUSION

This paper has deduced parallel navigation. The control objective is to keep the the pitch angle and yaw angle constant between the vehicle and the target, and it outperforms the PPN in terms of interception time. Under obstacles, cell decomposition algorithm is used to implement obstacle avoidance. Under uncertainties, interception can be implemented by using the estimation method. The parallel navigation is verified by using simulations, which can prove the efficiency of this method.

ACKNOWLEDGEMENT

This work was supported in part by the National Natural Science Foundation of China under Grant 61603172, in part by the Natural Science Foundation of Shandong Province under Grant BS2015DX018, in part by Science and Technology Development Program of Yantai City (Grant No. 2021XDHZ085).

(Received October 9, 2022)

REFERENCES

-
- [1] F. Belkhouche and B. Belkhouche: Ball interception by a mobile robot goalkeeper using the parallel navigation. In: Proc. 35th Int. Symp. on Robotics, Paris, WE14-145, 2004.
 - [2] F. Belkhouche and B. Belkhouche: Modified parallel navigation for ball interception by a wheeled mobile robot goalkeeper. *Advanced Robotics* 20 (2006), 429–452. DOI:10.1163/156855306776562260
 - [3] F. Belkhouche, B. Belkhouche, and P. Rastgoufard: Parallel navigation for reaching a moving goal by a mobile robot. *Robotica* 25 (2007), 63–74. DOI:10.1017/S0263574706002992
 - [4] S. K. Debnath, R. Omar, and S. Bagchi: Different Cell Decomposition Path Planning Methods for Unmanned Air Vehicles – A Review. John Wiley, New York 2021.
 - [5] J. W. Jung, B. C. So, and J. G. Kang: Expanded Douglas–Peucker polygonal approximation and opposite angle-based exact cell decomposition for path planning with curvilinear obstacles. *Appl. Sci.* 9 (2019), 638–654. DOI:10.3390/app9040638
 - [6] S. Knotek, K. Hengster-Movric, and M. Sebek: Distributed estimation on sensor networks with measurement uncertainties. *IEEE Trans. Control Systems Technol.* 29 (2020), 1997–2011. DOI:10.1109/TCST.2020.3026815
 - [7] B. Q. Ma: Research on synchronous control algorithm for multi ship parallel navigation. *Ship Science Technol.* 39 (2017), 28–30.
 - [8] M. Reza J. Harandi, S. A. Khalilpour, H. D. Taghirad and J. G. Romero: Adaptive control of parallel robots with uncertain kinematics and dynamics. *Mechanical Systems Signal Process.* 157 (2021), 1–12. DOI:10.1016/j.ymssp.2021.107693
 - [9] H. Myint and H. M. Tun: Analysis on guidance laws implementation based on parallel navigation time domain scheme. *Int. J. Scientific Res. Publ.* 8 (2018), 65–77. DOI:10.29322/ijsrp.8.8.2018.p80105
 - [10] E. Picard, E. Tahoumi, and F. Plestan: A new control scheme of cable-driven parallel robot balancing between sliding mode and linear feedback. *IFAC-PapersOnLine* 53 (2019), 9936–9943. DOI:10.1016/j.ifacol.2020.12.2708
 - [11] M. Rafie-Rad: Time-optimal solutions of parallel navigation and finsler geodesics. *Nonlinear Analysis: Real World Appl.* 11 (2010), 3809–3814. DOI:10.1016/j.nonrwa.2010.02.010
 - [12] V. Ferravant, E. Riva, M. Taghavi, and T. Bock: Dynamic analysis of high precision construction cable-driven parallel robots. *Mechanism Machine Theory* 2019 (2019), 54–64. DOI:10.1016/j.mechmachtheory.2019.01.023
 - [13] N. Schultz: Bats track diving mantises with parallel navigation. *J. Experiment. Biology* 212 (2009), 893–903. DOI:10.1242/jeb.030544
 - [14] N. A. Shneydor: Parallel navigation. *Missile Guidance and Pursuit* 9 (1998), 77–100.

- [15] C. d. Souza, P. Castillo, and B. Vidolov: Reactive drone pursuit and obstacle avoidance based in parallel navigation. In: IEEE 23rd International Conference on Intelligent Transportation Systems (2020), pp. 1–6.
- [16] J. Su: Research on the precision control algorithm for multi-ship parallel navigation track. *Ship Science Technol.* 41 (2019), 43–45.
- [17] J. Sun, H. Zhang, and Y. Wang: Dissipativity-based fault-tolerant control for stochastic switched systems with time-varying delay and uncertainties. *IEEE Trans. Cybernet.* 52, (2021), 10683–10694. DOI:10.1109/tcyb.2021.3068631
- [18] H. Sun, R. Madonski, and S. Li: Composite control design for systems with uncertainties and noise using combined extended state observer and Kalman filter. *IEEE Trans. Industrial Electronics* 69 (2021), 4119–4128. DOI:10.1109/TIE.2021.3075838
- [19] B. F. Wang, M. Iwasaki, and J. P. Yu: Command filtered adaptive backstepping control for dual-motor servo systems with torque disturbance and uncertainties. *IEEE Trans. Industrial Electronics* 29 (2021), 80–87. DOI:10.1109/tie.2021.3059540
- [20] Z. Xu, X. Zhou, and H. Wu: Motion planning of manipulators for simultaneous obstacle avoidance and target tracking: an RNN approach with guaranteed performance. *IEEE Trans. Industr. Electronics* 9 (2021), 71–79. DOI:10.1109/tie.2021.3073305
- [21] R. Yanushevsky: New guidance laws to implement parallel navigation. Aiaa Guidance, Navigation, Control Conference and Exhibit, 2013.
- [22] D. Y. Zhao, B. L. Si, and X. L. Li: Learning allocentric representations of space for navigation. *Neurocomputing* 453 (2021), 579–589. DOI:10.1016/j.neucom.2020.10.013

Shulin Feng, Corresponding author. School of Information and Electrical Engineering, Ludong University, Yantai 264025. P. R. China.

e-mail: fengshulin@ldu.edu.cn

Shuning Zhang, School of Information and Electrical Engineering, Ludong University, Yantai 264025. P. R. China.

e-mail: zhangshn0221@163 .com

Mingming Xu, School of Information and Electrical Engineering, Ludong University, Yantai 264025. P. R. China.

e-mail: hawkeagle57@163.com

Guanlong Deng, School of Information and Electrical Engineering, Ludong University, Yantai 264025. P. R. China.

e-mail: dglag@163.com